A stringent upper limit of the H_2O_2 abundance in the Martian atmosphere

Th. Encrenaz[1], T. K. Greathouse[2], B. Bézard[1], S. K. Atreya[3], A. S. Wong[3], M. J. Richter[4], and J. H. Lacy[2]

[1] LESIA, Observatoire de Paris, 92195 Meudon, France
[2] Department of Astronomy, University of Texas at Austin, RLM 15.308, C-1400, Austin, TX 78712-1083, USA
[3] The University of Michigan, Ann Arbor, MI 48109-2143, USA
[4] Department of Physics, One Shields Ave., University of California, Davis, CA 95616, USA

Abstract. Hydrogen peroxide H_2O_2 has been suggested as a possible oxidizer of the Martian surface. However, this minor species has never been detected. Photochemical models suggest that H_2O_2 and H_2O abundances should be correlated. We have searched for H_2O_2 in the northern atmosphere of Mars, on Feb. 2–3, 2001 (Ls = 112 deg), at a time corresponding to maximum water vapor abundance in the northern hemisphere. The TEXES high-resolution grating spectrograph was used at the NASA/Infrared Telescope Facility (IRTF). Individual lines of the H_2O_2 ν_6 band were searched for in the 1226–1235 cm^{-1} range (8.10–8.15 μm). Data were co-added for three different latitude sets: (1) full northern coverage (0–90 deg); (2) low northern latitudes (10–40 deg); (3) high northern latitudes (40–60 deg). From the absence of detectable H_2O_2 lines in each of the three co-added data sets, we infer an H_2O_2 2-σ upper limit of 9×10^{14} cm^{-2} in the first case, 1.2×10^{15} cm^{-2} in the second case, and 1.1×10^{15} cm^{-2} in the third case. These numbers correspond to mean water vapor abundances of 30 pr-μm, 20 pr-μm and 40 pr-μm at the time of our observations. Our lowest upper limit is eight times lower than the value derived by Krasnopolsky et al. (1997) in the southern hemisphere in June 1988 (Ls = 222 deg); the mean water vapor abundance corresponding to their observation was 10 pr-μm. Our lowest upper limit is between 2.5 and 10 times lower than the values predicted by global photochemical models, also calculated for a mean H_2O abundance of 10 pr-μm. In view of this, we have developed a new photochemical model which takes into account the actual geometry of the observations and the corresponding conditions of the water vapor abundance, dust and temperature in the Martian atmosphere, inferred from the MGS/TES data. Assuming an eddy diffusion coefficient of 10^7 cm^2 s^{-1} in the lower atmosphere, the calculated H_2O_2 abundance is only a factor 1.5 greater than the observed upper limits.

Key words. planets and satellites: individual: Mars – infrared: solar system

1. Introduction

Photochemical models of the Martian atmosphere predict the formation of hydrogen peroxide H_2O_2 (Parkinson & Hunten 1972; Krasnopolsky 1986; Atreya & Gu 1994). This molecule is believed to be formed from the combination of two HO_2 radicals, which result from a reaction involving H, O_2 and CO_2:

$$H + O_2 + CO_2 \longrightarrow HO_2 + CO_2$$
$$HO_2 + HO_2 \longrightarrow H_2O_2 + O_2$$
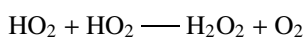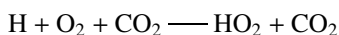
H_2O_2 is subsequently photodissociated into OH through the reaction:

$$H_2O_2 + h\nu \longrightarrow 2 \text{ OH}.$$
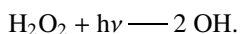
Following the results of the Viking Labeled Released life science experiment (Levin & Straat 1988), it was suggested that H_2O_2 in the Martian soil might be responsible for the positive response of that experiment (Huguenin 1982). H_2O_2 might thus be the very active, oxidizing species responsible for the absence of organic compounds on the Martian surface (Klein et al. 1992).

Theoretical vertical profiles of H_2O_2 have been calculated by many authors including Kong & McElroy (1977), Krasnopolsky & Parshev (1979), Shimazaki (1989), Krasnopolsky (1993, 1995), Atreya & Gu (1994), Nair et al. (1994), and Clancy & Nair (1996). As pointed out by Barth et al. (1992), the amount of H_2O_2 is difficult to estimate, because of the short time constants of its production and loss reactions, shorter than the duration of daylight. The above photochemical models are "global", i.e. they represent seasonal and diurnal average conditions. They predict an H_2O_2 vertical

profile which strongly decreases as the altitude increases, with an effective scale height of about 5 km (Krasnopolsky 1986), i.e. half the mean atmospheric scale height, with a column density in the range of 10^{15}–10^{16} cm^{-2}. These numbers correspond to mean mixing ratios in the range of 4×10^{-9}–4×10^{-8}, or to surface mixing ratios in the range 8×10^{-9}–8×10^{-8}.

Due to the large intensities of several H$_2$O$_2$ fundamental bands, infrared spectroscopy appears to be well suited for the search for hydrogen peroxide. In view of the weak surface pressure on Mars, coupled with the low expected mixing ratio of H$_2$O$_2$, high spectral resolution, with a resolving power higher than 10^4, is essential. The best candidate is the ν_6 fundamental band centered at 1266 cm^{-1} (7.9 μm). Other strong fundamental bands of H$_2$O$_2$ appear at 317 cm^{-1} (ν_4) and 3608 cm^{-1} (ν_5), but in the first case no high-resolution Martian data exist, and in the second case, the band falls within a strong mixture of CO$_2$ overtone and combination bands. The first attempt to detect the ν_6 band was achieved by Bjoraker et al. (1987) in October 1986, using a cooled grating in combination with a Fourier Transform spectrometer at the Kitt Peak solar telescope ($R = 10^4$), who derived, for the H$_2$O$_2$ mean mixing ratio, an upper limit of a few times 10^{-7}. The second attempt was made by Krasnopolsky et al. (1997) in June 1988, using the Goddard post-disperser associated with the Fourier Transform spectrometer mounted at the Kitt Peak solar telescope ($R = 1.2 \times 10^5$). A 2-σ upper limit of 7.5×10^{15} cm^{-2} was obtained for the H$_2$O$_2$ column density, corresponding to a mean mixing ratio of 3×10^{-8}. As pointed out by the authors, this value was close to the predictions given by photochemical models.

The production mechanism of H$_2$O$_2$, through the combination of HO$_2$ radicals, suggests a strong correlation between the H$_2$O and H$_2$O$_2$ abundances; all photochemical models of Mars predict this correlation. Hydrogen peroxide should thus be searched for at a time and location corresponding to a maximum of the water vapor abundance. As shown by the Viking MAWD experiment (Jakosky & Haberle 1992), as well as more recent measurements by the TES infrared spectroscopy experiment aboard the Mars Global Surveyor (Smith 2002), the H$_2$O vapor content ranges from less than 1 pr-μm, at and near the winter polar cap, up to a maximum value as high as 80 pr-μm at high northern latitudes in the beginning of northern summer (Ls = 110–120 deg), with another less pronounced local maximum of 15 pr-μm at high southern latitudes at the end of the southern spring (Ls = 265–270 deg). The upper limit obtained by Krasnopolsky et al. (1997) was derived in the southern hemisphere of Mars, for an areocentric longitude Ls of 222 deg. The corresponding water vapor column density was 10 pr-μm.

In this paper, we present a new attempt to detect the H$_2$O$_2$ ν_6 band, using a high-resolution grating spectrograph (TEXES) at the NASA Infrared Telescope Facility (IRTF). The data were obtained over the northern hemisphere of Mars, at the time and location corresponding to maximum water vapor abundance (Ls = 112 deg). No H$_2$O$_2$ spectral signature was detected. Our derived upper limit, however, is significantly below the previous measurements, as well as the predictions of current "global" photochemical models. Section 2 describes the observations. In Sect. 3, we show the spectral modelling and the comparison of our data with synthetic spectra. In Sect. 4, our results are discussed and an attempt is made to reconcile them with a new photochemical model.

2. Observations

Observations of Mars were made on February 2–3, 2001, with the Texas Echelon Cross Echelle Spectrograph (TEXES) mounted at the 3-m NASA/Infrared Telescope Facility (IRTF). TEXES is a mid-infrared spectrograph operating between 5 and 25 μm with several modes, which can achieve a spectral resolving power up to 10^5 (Lacy et al. 2002). We used the high resolution, cross dispersed mode, with a 1.1×6 arcsec slit. Our data were recorded in the 1226–1236 cm^{-1} spectral range. Our spectral resolution was 0.017 cm^{-1}, corresponding to a resolving power of 7.2×10^4.

At the time of our observations, the diameter of Mars was 6.4 arcsec. The areocentric longitude was 112 deg, corresponding to the beginning of northern summer. The latitudes of the sub-solar point and the sub-terrestrial point were +24 deg and +12 deg respectively. Conditions were thus optimized for observing a maximum water vapor abundance in the northern hemisphere. Mars was approaching the Earth at −17.5 km s^{-1}, corresponding to a Doppler shift of 0.072 cm^{-1}.

Data were recorded simultaneously along the slit, with a pixel size of 0.3 arcsec. Because the data were taken in connection with a Jupiter run, the slit angle was not aligned along the Martian central meridian (North polar angle of Mars: +37 deg) but with an angle corresponding to the Jupiter north polar angle (−12 deg). On Feb. 2, two spectra of 3.5 min integration each were recorded with the slit in a fixed position, including the Martian center and the northern hemisphere. We co-added all pixels corresponding to northern latitudes in the range 10N–40N (spectrum S1). On Feb. 3, two data sets of 4 min integration each were recorded with the slit scanning the northern hemisphere. The geometry corresponding to one of these maps is shown in Fig. 1. Our first objective was to look at individual spectra corresponding to specific locations on the Martian disk, in order to search for possible variations of the H$_2$O$_2$ abundance. As H$_2$O$_2$ was not detected, we co-added all data in different latitude ranges: 0-90N (spectrum S2), 10N–40N (S3) and 40–60N (S4). The third case was chosen to isolate an area where, according to the Viking measurements (Jakosky & Haberle 1992) the water vapor content is expected to be higher. Table 1 summarizes the characteristics of the Mars spectra, their corresponding atmospheric parameters and the derived H$_2$O$_2$ upper limits.

The presence of a strong background emission at mid-IR wavelengths makes the data calibration especially important. Calibration of the TEXES spectra follows the radiometric method commonly used for millimeter and submillimeter observations (Rohlfs 1986). Calibration frames consisting of 3 measurements (black chopper blade, sky and low emissivity chopper blade) are systematically taken before each observing sequence, and the difference (black – sky) is taken as a flat field (a complete description of the procedure can be found in Lacy et al. 2002). If the temperatures of the black blade, the telescope and the sky are equal, this method corrects both telescope and

Table 1. Summary of Mars spectra and corresponding H_2O_2 upper limits.

| Spectrum	S1	S2	S3	S4
Date	Feb. 2, 01	Feb. 3, 01	Feb. 3, 01	Feb. 3, 01
Time	16:32 UT	16:47 UT	16:47 UT	16:47 UT
Obs. time (s)	2332	1134	486	648
Lat. range	10N–40N	0–90N	10N–40N	40N–60N
H_2O (pr-μm)	20	30	20	40
Ts (K)	240	230	250	230
$T(z = 0$ km) (K)	235	225	235	225
$T(z = 20$ km) (K)	180	170	180	170
Airmass factor	1.25	1.6	1.25	1.6
q_{H2O2} (mean)	6×10^{-9}	4×10^{-9}	9×10^{-9}	6×10^{-9}
N_{H2O2} (cm^{-2})	1.2×10^{15}	9×10^{14}	1.8×10^{15}	1.1×10^{15}

Fig. 1. Geometry of the observations on Feb. 3, 2001. The diameter of Mars is 6.4 arcsec. The black circle indicates the sub-solar point, and the open circle the sub-terrestrial point. The slit size is 1.1×6 arcsec. Pixels were selected according to different latitude ranges (see Table 1).

atmospheric transmissions. The atmospheric correction, however, is not complete for all the terrestrial atmospheric lines, partly because these lines are not all formed at the same atmospheric levels, and thus have different temperatures.

Figure 2a shows the full Mars spectrum between 1226.7 and 1235.4 cm^{-1}, corresponding to the first selection S1 (low northern latitudes). This spectrum is a combination of 14 individual spectra, each having a bandwidth of about 0.8 cm^{-1}, corresponding to different orders of the spectrometer. It can be seen that the strongest terrestrial atmospheric lines, due to CH$_4$, are still visible, as shown by the synthetic atmospheric transmission spectrum shown in Fig. 2d. Apart from these telluric signatures, all the spectral features appearing in the Mars spectrum can be attributed to CO$_2$ isotopic lines, as illustrated by a comparison of the Mars spectrum with a synthetic CO$_2$ spectrum of Mars (Fig. 2c). Figure 2b shows a synthetic spectrum of H$_2$O$_2$ on Mars calculated for a column density of 2×10^{16} cm^{-2} (mean mixing ratio of 10^{-7}). As will be discussed below, a careful examination shows that none of the H$_2$O$_2$ transitions is detectable in the Mars spectrum. In Figs. 2b and c, the synthetic spectra have been shifted by 0.072 cm^{-1} to account for the Doppler shift.

Figure 3 displays 4 different orders of the Martian spectra, which correspond to spectral ranges where the best H$_2$O$_2$ line candidates can be searched for. In the case of S1 (Feb. 2, 01), the signal to noise ratio in the continuum (between 50 and 100) is higher than in the data set used by Krasnopolsky et al. (1997), but our spectral resolving power is about twice lower. However, our calculations have shown that this spectrum does not lead to the lowest H$_2$O$_2$ upper limit. Indeed, some oscillations are visible in the continuum, especially around 1234.0–1234.2 cm^{-1} (Fig. 3c). These features, which are not present in the other spectra taken on Feb. 3 (Fig. 4c), could be associated with imperfect flat-fielding, or might be associated with small emissivity fluctuations at the surface of Mars. In the case of the Feb. 3, 01 data, the best H$_2$O$_2$ upper limit is achieved, as expected, in the spectrum corresponding to the longest integration time.
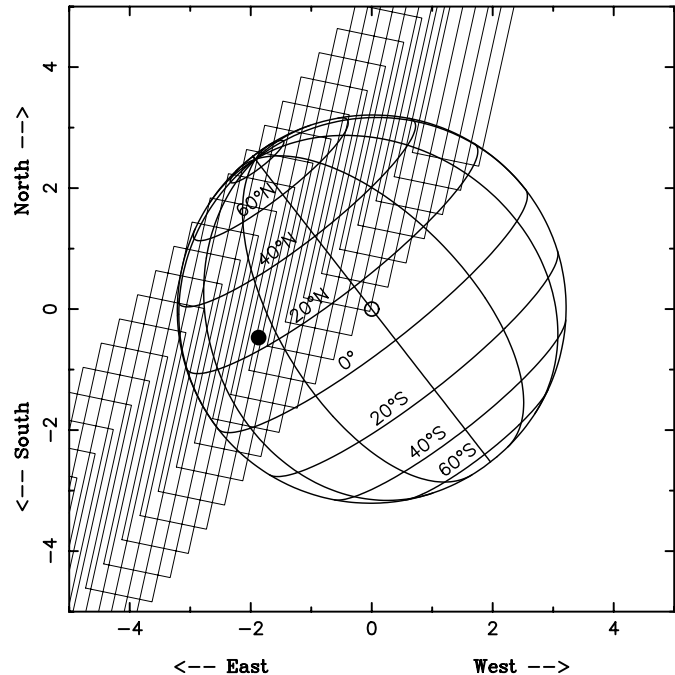
3. Modelling and interpretation

3.1. Atmospheric modelling

We first attempted to determine the atmospheric parameters which would provide a good fit of the CO$_2$ lines. We determined the mean surface temperature from the mean continuum level inferring the values listed in Table 1. Local variations over the Martian disk, measured in the individual pixels along the slit, indicate a maximum temperature of 260 K, in global agreement with the predictions of the global climate models (Forget et al. 1999) as well as the recent TES results (Smith et al. 2001). We chose a mean surface pressure of 7 mbar, in agreement with Smith (2002).

Two sets of CO$_2$ isotopic lines are present in our data: a relatively "strong" band of $^{12}C^{16}O^{18}O$ (10002–00001) shows for the individual lines a typical depth of 25–30 percent. In a weaker band of $^{12}C^{16}O^{18}O$ (11102–01101) and in the $^{13}C^{16}O^{18}O$ (10002–00001) band, the typical depth of the lines is about 5–10 percent. All CO$_2$ absorption features in the Martian spectrum are relatively weak, which indicates that they are formed in the lower atmosphere. Assuming a terrestrial value for the $^{12}C/^{13}C$ Martian ratio (Nier & Mc Elroy 1977), we have used the 3 sets of CO$_2$ lines to constrain the temperature lapse rate in the lower Martian atmosphere, which we have parametrized by the mean atmospheric temperature at an altitude of 20 km (T_{20}) and the atmospheric temperature at $z = 0$ km (T_0). A good fit of the depth of all CO$_2$ Martian lines is achieved with the values of T_{20} and T_0 given in Table 1. These values are consistent with GCM predictions (Forget et al. 1999) and recent TES determinations
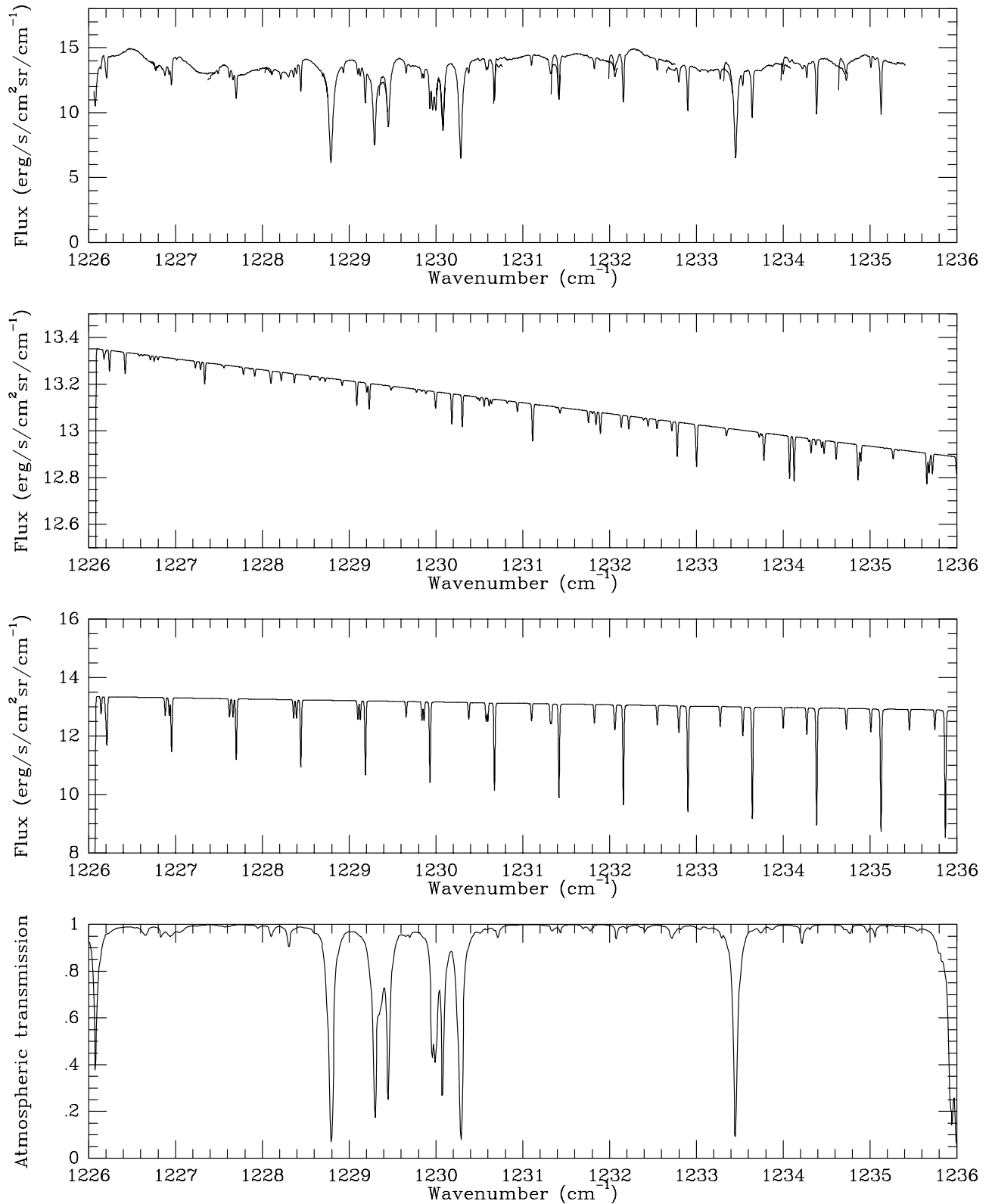
Fig. 2. From top to bottom: **a)** The spectrum of Mars at low northern latitudes (10N–40N) between 1226 and 1236 cm^{-1} (spectrum S1). The spectral resolution is 0.017 cm^{-1}. **b)** A synthetic spectrum of H$_2$O$_2$ under the Martian conditions (see Sect. 3), corresponding to a column density of 2×10^{16} cm^{-2} (mean mixing ratio of 10^{-7}). **c)** A synthetic spectrum of CO$_2$ under the Martian conditions. **d)** A synthetic model of the terrestrial atmospheric transmission at Mauna Kea, for a terrestrial water content of 1 pr-mm and a zenith angle of 45 deg. The Mars spectrum is dominated by Martian CO$_2$ and incompletely cancelled telluric CH$_4$, in addition to broad features due to imperfect flat-fielding.
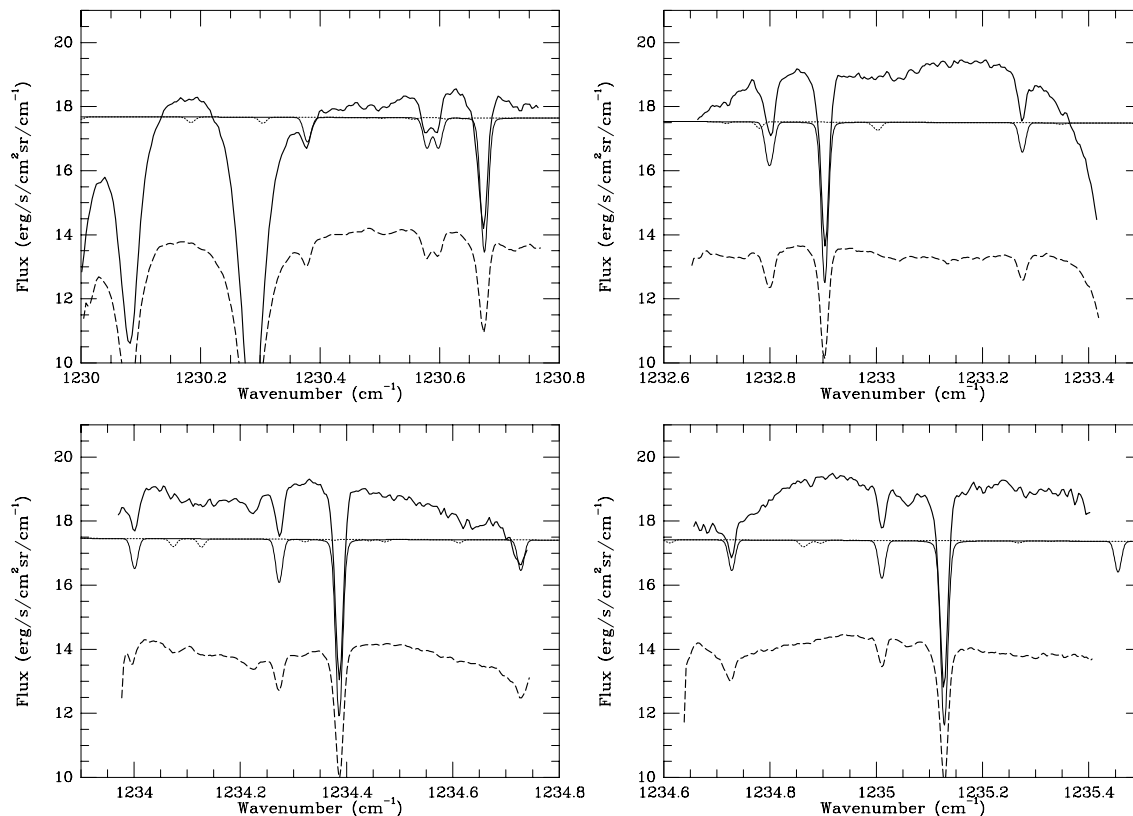
Fig. 3. The spectra of Mars at low latitudes (10N–40N) in 4 different orders: **a)** 1230–1230.8 cm^{-1}; **b)** 1232.6–1233.5 cm^{-1}; **c)** 1233.9–1234.8 cm^{-1}; **d)** 1234.6–1235.5 cm^{-1}. Bold solid line: spectrum S3 (see Table 1); bold dashed line: spectrum S1; thin solid line: synthetic model with CO$_2$ only (shifted by 0.072 cm^{-1}); thin dotted line: synthetic model with H$_2$O$_2$ only, shifted by 0.072 cm^{-1} (column density of 2×10^{16} cm^{-2}, corresponding to a mean mixing ratio of 10^{-7}). The spectral resolution is 0.017 cm^{-1}. The continuum level defines the value of Ts (see Table 1). The continuum is stronger in S3 because this pixel selection corresponds to an area closer to the subsolar point (see text and Fig. 1).

(Smith et al. 2001). We have to notice, however, that the values Ts, T_0 and T_{20} may have little physical meaning. We know that Ts exhibits strong fluctuations over the Martian disk. In addition, we have not considered possible effects associated to dust opacity. This approximation looks reasonable because the atmospheric dust content was low at the time of our observations (Smith et al. 2001) and because the observed Martian CO$_2$ lines are weak enough to be unaffected by scattering. For these reasons, we only use Ts, T_0 and T_{20} as ad hoc parameters for realistic modelling of the H$_2$O$_2$ absorption. These approximations are acceptable because (1) in view of its small scale height, H$_2$O$_2$ is expected to be concentrated near the surface, so the H$_2$O$_2$ line formation does not depend upon the Martian atmospheric structure above an altitude of 20 km, and (2) the H$_2$O$_2$ lines occur in the same spectral region as the CO$_2$ lines.

Figure 3 shows the synthetic absorption spectrum of H$_2$O$_2$ and CO$_2$, calculated at a resolution of 0.017 cm^{-1} and shifted with respect to the Martian spectrum by 0.072 cm^{-1} (to account for the Doppler shift), for comparison with the Martian data at low northern latitude (S1 and S3). It can be seen that the depths of the CO$_2$ lines are well reproduced by the synthetic spectrum. It also appears that no H$_2$O$_2$ line is detected in the Mars data.

In order to improve our upper limit on the H$_2$O$_2$ abundance, we have selected all H$_2$O$_2$ line positions which were free of CO$_2$ and terrestrial absorptions. Six lines filled this

criterion: taking into account the Doppler shift, they had to be searched for at 1230.18, 1233.00, 1233.78, 1234.08, 1234.13 and 1234.87 cm^{-1}. Spectra around these frequencies, taken over a bandwidth of 0.07 cm^{-1}, were co-added and compared to the synthetic model. From the absence of detection, by fitting a second-order polynomial, we infer from the S1 spectrum a 2-σ upper limit of 1.2×10^{15} cm^{-2}, corresponding to a mean mixing ratio of 6×10^{-9}, or, assuming a scale height of 5 km, a surface mixing ratio of 1.2×10^{-8}. From the S3 spectrum, a 2-σ upper limit of 1.8×10^{15} cm^{-2} is inferred (see Table 1).

Figure 4 shows the Mars spectra of Feb. 3, 01 corresponding to the two other selections S2 (0–90N) and S4 (40N–60N), in the same spectral orders as in Fig. 3. Again, there is no evidence for an H$_2$O$_2$ signature.

At high latitudes lower surface temperatures cause the observed decrease in continuum flux. Surprisingly, the depths of the CO$_2$ lines are remarkably similar to those shown in the first case. A plausible interpretation is the following: the atmospheric temperature is less variable than the surface temperature over the Martian disk, so that the line contrast, for the same emission angle, would be stronger near the disk center (not far from the sub-solar point) than at high northern latitude; however this effect is counterbalanced by the airmass factor, stronger toward the limb, which tends to increase this contrast. Using the same co-addition method as described above and a
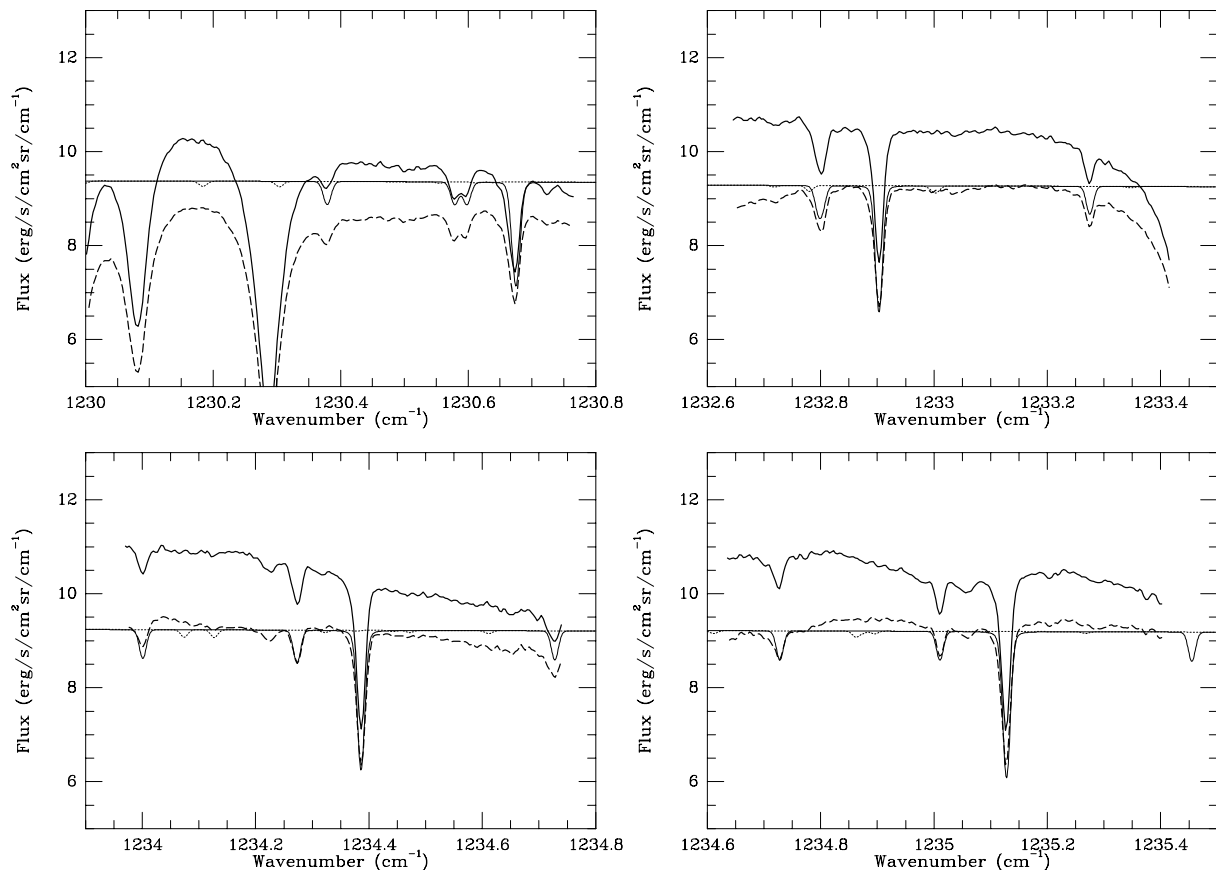
Fig. 4. The spectra of Mars S4 (40N–60N, bold solid line) and S2 (0–90N, bold dashed line) in 4 different orders (see Fig. 2). Thin solid line: synthetic model with CO_2 only (shifted by 0.072 cm^{-1}); thin dotted line: synthetic model with H_2O_2 only, shifted by 0.072 cm^{-1} (column density of 2×10^{16} cm^{-2}, corresponding to a mean mixing ratio of 10^{-7}). The spectral resolution is 0.017 cm^{-1}.

second-order polynomial fit, we infer, at 0–90N (S2), an upper limit of 9×10^{14} cm^{-2}, corresponding to a mean mixing ratio of 4×10^{-9}. For the high latitude selection S4, we infer an H_2O_2 upper limit of 1.1×10^{15} cm^{-2}, i.e. a mean mixing ratio of 6×10^{-9} (Table 1 and Fig. 5).

4. Discussion and photochemical modelling

Our upper limit for the full northern hemisphere (0–90N) corresponds to a mean water vapor abundance of about 30 pr-μm (Smith 2002). Our result is eight times lower than the result obtained by Krasnopolsky et al. (1997), which corresponds to a water vapor content of 10 pr-μm. Our upper limit concerning the high northern latitudes, about 6 times lower than Krasnopolsky et al.'s value, refers to a mean H_2O abundance of about 40 pr-μm.

As pointed out by the authors, the upper limit derived by Krasnopolsky et al. (1997) was still consistent with the predictions from global photochemical models: 2.2×10^{15} cm^{-2} (Shimazaki 1989); 3.8×10^{15} cm^{-2} (Krasnopolsky 1993); 2.4×10^{15} cm^{-2} (Nair et al. 1994); 10^{16} cm^{-2} (Atreya & Gu 1994); 4–6×10^{15} cm^{-2} (Krasnopolsky 1995). The upper limits derived in the present study are significantly lower than all these estimates. It should be stressed that most of these models represent diurnal and seasonal averages, and correspond to a mean water vapor abundance of 10 pr-μm. A time-dependent
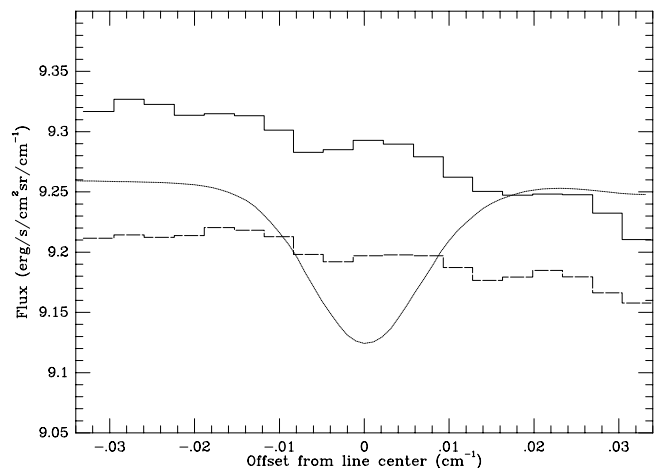

Fig. 5. The S2 and S4 spectra of Mars of Feb. 3, 01 (histograms) co-added in 6 spectral intervals of 0.07 cm^{-1} each, centered on H_2O_2 line frequencies (see text). Solid line: S4 (40N–60N); long-dashed line: S2 (0–90N). Dotted line: the corresponding synthetic spectrum calculated with H_2O_2 only, shifted by 0.072 cm^{-1} (H_2O_2 column density of 2×10^{16} cm^{-2}, corresponding to a mean mixing ratio of 10^{-7}). The spectral resolution is 0.017 cm^{-1}.

photochemical model, however, was developed by Clancy & Nair (1996). In their paper, the authors do not indicate the total column density of H_2O_2 nor its vertical distribution, but they

show the H$_2$O$_2$ mixing ratio as a function of the areocentric longitude Ls for two altitude levels, 20 km ($P = 0.9$ mbar) and 40 km ($P = 0.08$ mbar). If we assume, as in Krasnopolsky (1986), a H$_2$O$_2$ vertical distribution characterized by a scale height of 5 km, we can derive its mixing ratio at the surface and its total column density. For Ls = 112 deg, Clancy and Nair infer an H$_2$O$_2$ mixing ratio of about 1.5×10^{-9} at an altitude of 20 km. This translates into a surface mixing ratio of 7×10^{-8}, corresponding to a mean mixing ratio of 3.5×10^{-8} and a total column density of 7×10^{15} cm^{-2}. Our lowest upper limit is eight times lower than this value.

Comparison of the observed H$_2$O$_2$ abundance with the published photochemical models is a good starting point. However, none of these models represent the geometry, season or the insolation of the reported observations. Neither are the appropriate Martian atmospheric conditions, including the amount of water vapor and temperature structure, taken into account. These factors, as well as certain atmospheric parameters such as the eddy diffusion coefficient and the dust opacity, and uncertainties in chemical kinetics have an effect on the model results, including possible reduction in the H$_2$O$_2$ abundance relative to the global average model. We present below the results of a new model which is in better agreement with our observations.

For the period and geometry of observations, the amount of water varied from 12 pr-μm at 10N to a little over 60 pr-μm at 80N, as measured from infrared spectroscopy by the TES instrument (Smith 2002), whereas the global models all assume 10 pr-μm. As mentioned above, the H$_2$O$_2$ abundance is strongly correlated with the water vapor abundance through the production of HO$_2$ radicals. In the present study we take the appropriate water vapor abundance and calculate our results at intervals of 10 degrees in latitude. Surface temperature from this work and the MGS/TES derived temperatures for the higher elevations (Smith et al. 2001) are used in the present study.

No planet-encircling dust storms were seen at the time of our observations. As mentioned above, the dust opacity τ_D was very low, varying from 0.05 to 0.1 (Smith et al. 2001). By reducing τ_D in the UV from 0.4 (the value usually taken in global models) to 0.2, the H$_2$O$_2$ abundance reduces by about 20 percent.

The choice of vertical mixing has a greater effect, however. In the models of Atreya & Gu (1994), $K = 10^6$ cm^2 s^{-1} is used for the lower atmosphere where most of the H$_2$O$_2$ is produced. Increasing K by a factor of 10 can reduce the H$_2$O$_2$ abundance by a factor of 2. The eddy diffusion coefficient is highly uncertain in the lower atmosphere of Mars; however, $K = 10^7$ cm^2 s^{-1} appears to be well within the realm of available observational constraints.

The choice of rate constants of key chemical reactions has a noticeable effect on the H$_2$O$_2$ abundance. Recently, the self-reaction of HO$_2$ radicals that produces H$_2$O$_2$ has been measured at the low temperatures appropriate to the Martian photochemical regime (Christensen et al. 2002). For example, at 200 K, the rate constant is a factor of 3 lower than the value assumed in prvious models. The resulting H$_2$O$_2$ abundance is about 25 percent smaller with the new measured rate. The reaction HO$_2$ + OH is an important removal mechanism for HO$_2$,

and the uncertainty in its rate constant is as much as a factor of 3 (DeMore et al. 1997). Using the upper bound (rather than the central value) for this rate constant can reduce the H$_2$O$_2$ abundance by another 25 percent.

With the above mentioned changes, the model H$_2$O$_2$ column abundance at the surface of Mars is found to be 1.3×10^{15} cm^{-2} when averaged over 10N–40N, and 1.5×10^{15} cm^{-2} when averaged between 40N and 60N. These values are not much above our upper limits for these cases (only a factor about 1.5). It is interesting to note that for the period and region of observations, an eddy diffusion coefficient larger than 10^7 cm^{-2} s^{-1} in the lower atmosphere of Mars is most favorable for reconciling the model H$_2$O$_2$ abundance with the measured upper limit.

Many other factors than the ones discussed above can reduce the model H$_2$O$_2$ abundance even more. For example, there may be important loss of HO$_2$ or H$_2$O$_2$ to the surface of Mars. Dynamics, including transport to the nightside, can also reduce the H$_2$O$_2$ abundance. In the models of Clancy & Nair (1996), the expected maximum of the H$_2$O$_2$ abundance does not occur for Ls = $110-120$ deg, as is the case of H$_2$O, but for Ls = 180 deg. This time lag is probably due to condensation/transport effects of H$_2$O: when the water vapor content is maximum, condensation at low altitude may occur, and less H$_2$O water vapor is available at higher altitudes where most of the photochemistry takes place.

The robustness of our photochemical model may be tested by calculating the O$_2$ 1.27 μm dayglow intensity from the ozone abundance in the model. We find that our model produces an O$_2$ 1.27 μm dayglow intensity within a factor 2 of the value observed by Krasnopolsky in 1999 at Ls = 112 deg and under similar conditions of H$_2$O abundance, dust opacity and temperature as our H$_2$O$_2$ observations (Krasnopolsky & Bjoraker 2000; V. Krasnopolsky, personal communication 2002). By way of comparison, the photochemical model of Clancy & Nair (1996) gives ozone concentrations that result in a larger discrepancy in the O$_2$ dayglow intensity (Krasnopolsky & Bjoraker 2000).

In summary, this work demonstrates that observational constraints combined with a complete photochemistry-dynamics model would be helpful for a better understanding of the composition, structure and evolution of the Martian atmosphere.

References

Atreya, S. K., & Gu, Z. 1994, J. Geophys. Res., 99, 13133

Barth, C. A., Stewart, I. F., Bougher, S. W., et al. 1992, Aeronomy of the current Martian atmosphere, in Mars, ed. H. H. Kieffer, B. M. Jakosky, C. W. Snyder, & M. S. Matthews (University of Arizona Press), 1054

Bjoraker, G. L., Mumma, M. J., Jenning, D. E., & Widemann, G. R. 1987, Bull. Am. Astron. Soc., 19, 818

Christensen, L. E., Okumura, M., Sander, D. M., et al. 2002, Geophys. Res. Letters, in press

Clancy, R. T., & Nair, H. 1996, J. Geophys. Res., 101, 12785.

DeMore, W. B., Sander, D. M., Golden, R., et al. 1997, Chemical kinetics and photochemical data for use in stratospheric modeling, evaluation number 12, 1997

Forget, F., Hourdin, F., Fournier, R., et al. 1999, J. Geophys. Res., 104, 24155

Huguenin, R. L. 1982, J. Geophys. Res., 87, 10069

Jakosky, B. M., & Haberle, R. M. 1992, The seasonal behavior of water on Mars, in Mars, ed. H. H. Kieffer, B. M. Jakosky, C. W. Snyder, & M. S. Matthews (University of Arizona Press), 1054

Klein, H. P., Horowitz, N. H., & Biemann, K. 1992, The search for extant life on Mars, in Mars, ed. H. H. Kieffer, B. M. Jakosky, C. W. Snyder, & M. S. Matthews (University of Arizona Press), 1221

Kong, T. Y., & McElroy, M. B. 1977, Icarus, 32, 168

Krasnopolsky, V. A. 1986, Photochemistry of the atmospheres of Mars and Venus (Springer-Verlag)

Krasnopolsky, V. A. 1993, Icarus, 101, 303

Krasnopolsky, V. A. 1995, J. Geophys. Res., 100, 3263

Krasnopolsky, V. A., & Parshev, V. A. 1979, P&SS, 27, 113

Krasnopolsky, V. A., & Bjoraker, G. L. 2000, J. Geophys. Res., 105, E8, 20179

Krasnopolsky, V. A., Bjoraker, G. L., Mumma, M. J., & Jennings, D. E. 1997, J. Geophys. Res., 102, 6525

Lacy, J. H., Richter, M., Greathouse, T. K., et al. 2002, Pub. Ast. Soc. Pac., 114, 153

Levin, G. V., & Straat, P. A. 1988, in The NASA Mars Conf., ed. B. Reiber (Univelt, San Diego), 187

Nair, H., Allen, M., Anbar, D., & Yung, Y. L. 1994, Icarus, 111, 124

Nier, A. O., & Mc Elroy, M. B. 1977, J. Geophys. Res., 82, 4341

Parkinson, T. D., & Hunten, D. M. 1972, J. Atm. Sci., 29, 1380

Rohlfs, K. 1986, Tools of Radio-Astronomy (Springer-Verlag)

Shimazaki, T. 1989, J. Geomagn. Geoelectr., 41, 273

Smith, M. D. 2002, J. Geophys. Res., in press

Smith, M. D., Pearl, J., Conrath, B., J., & Christensen, P. R. 2001, J. Geophys. Res., 28, 4263